

# Impact of sulfur concentration on morphological, optical, electrical and thermoelectrical properties of nanostructured MoO<sub>3</sub> thin films

M. Adelifard<sup>1</sup> · M. Jahandoost<sup>1</sup>

Received: 19 October 2015 / Accepted: 30 January 2016 / Published online: 3 February 2016  
© Springer Science+Business Media New York 2016

**Abstract** We have investigated the effect of sulfur concentration ( $[S]/[Mo] = 0\text{--}10$  at.%) on nanostructural, optical and electrical properties of MoO<sub>3</sub> thin films grown on glass substrate by spray pyrolysis technique. X-ray diffraction analysis showed that the films were crystallized with mixed structures of MoO<sub>3</sub> orthorhombic and MoS<sub>2</sub> hexagonal structure. According to FESEM images, the studied films have a sponge-type structure on the order of nanometers. Optical measurements revealed that two distinct inflexions indicative two transitions correspond to MoO<sub>3</sub>/MoS<sub>2</sub> phases in agreement with the XRD analysis. The Hall effect and thermoelectric measurements have shown p-type conductivity, and the free hole density increases with increasing sulfur to molybdenum ratio, in agreement with reflectance spectra of the layers. The obtained value of Seebeck coefficient for MoO<sub>3</sub> film with  $[S]/[Mo]$  ratio of 8 at.% was as high as 169  $\mu\text{V}/\text{K}$ .

## 1 Introduction

Transition metal oxides because of their physical and chemical properties have been the focus of much attention in view of their scientific and technological applications. Among these oxides, Molybdenum trioxides, MoO<sub>3</sub>, with a layer-type structure and interesting physical properties has been widely studied in recent years. MoO<sub>3</sub> finds application as a cathode material in the development of high-energy density solid-state micro batteries, imaging devices,

smart windows, gas sensors, supported catalysts and lubricants [1–3].

MoO<sub>3</sub> thin films exist in three phases namely: orthorhombic MoO<sub>3</sub> ( $\alpha$ -MoO<sub>3</sub>) and two metastable phases hexagonal MoO<sub>3</sub> ( $\beta$ -MoO<sub>3</sub>) and monoclinic MoO<sub>3</sub> ( $\gamma$ -MoO<sub>3</sub>). The orthorhombic phase ( $\alpha$ -MoO<sub>3</sub>) has a layered structure, which consists of double layers of MoO<sub>6</sub> octahedral. Various thin film deposition techniques such as thermal evaporation [4], sputtering [5], chemical vapor deposition (CVD) [6], spray pyrolysis deposition (SPD) [7, 8], electrodeposition [9] and flash evaporation [10] were employed for growth of molybdenum oxide thin films.

Among all these techniques, SPD is the promising one, because of its simplicity and the facility for cost effective large area deposition, with no need of any sophisticated instrumentation. A few attempts have been made to preparation this compound. Bouzidi et al. [7], investigated the effect of substrate temperature on the structural and optical properties of MoO<sub>3</sub> thin films prepared by spray pyrolysis in the temperature range from 200 to 300 °C. They estimated band gaps between 3.14 and 3.34 eV for these layers. Characterization of MoO<sub>3</sub> with the two phase's  $\alpha$  and  $\beta$  in each of the films and the study of surface morphology and optical properties of molybdenum oxide have been done by the spray pyrolysis method [8]. Although there have been little theoretical and experimental studies on the structural, electrical, and optical properties of molybdenum oxide crystals, to the basis of our knowledge, no real authentic information was available relative to nature of structural, optical, electrical and thermoelectrical of sulfur content MoO<sub>3</sub> thin films deposited by chemical spray pyrolysis technique.

In the present investigation, thin film of MoO<sub>3</sub> was deposited at atmospheric pressure on glass substrate. Also, S<sup>2-</sup> ion has been selected to study the effect of doping on

✉ M. Adelifard  
adelifard@du.ac.ir

<sup>1</sup> School of Physics, Damghan University, Damghan, Iran

the structural, morphological, optical, electrical and thermoelectrical properties of MoO<sub>3</sub> thin films. This selection is based on the electron valence and ionic radius values of O<sup>2-</sup> and S<sup>2-</sup>, respectively. Oxygen and sulfur are similar in many physical and chemical properties, due to a similar structure of the electronic shell. Therefore, S<sup>2-</sup> can substitute for O<sup>2-</sup> ion. Such substitution has been reported to changes optical and electrical properties in SPD films [11].

## 2 Experimental descriptions

### 2.1 Preparation of MoO<sub>3</sub> and Sulfur content MoO<sub>3</sub> thin films

Pure MoO<sub>3</sub> thin film and S-content MoO<sub>3</sub> thin films were deposited onto glass substrate using chemical spray pyrolysis technique. In order to prepare the basis spray solution for any sample, 0.01 M (0.618 g) of ammonium molybdate tetrahydrate ((NH<sub>4</sub>)<sub>6</sub>Mo<sub>7</sub>O<sub>24</sub>·4H<sub>2</sub>O) was added to 50 ml double distilled water. Then thiourea (CS(NH<sub>2</sub>)<sub>2</sub>) as the source for sulfur with four various S to Mo molar ratios of 4, 6, 8 and 10 was dissolved into the basis solution. The calculation of the amount of CS(NH<sub>2</sub>)<sub>2</sub> (? g) with S/Mo = 8 at.% in solution is described in the following:

$$[S]/[Mo = 0.01 M] = 8 \rightarrow [S] = 0.08 M \quad (1)$$

$$\begin{aligned} &0.08 \text{ (mol/1000 ml)} \times 50 \text{ ml} \\ &\times \text{(Molar Mass of CS(NH}_2\text{)}_2 = 76.12 \text{ g mol}^{-1}\text{)} \\ &= 0.305 \text{ g} \end{aligned} \quad (2)$$

The final solution was stirred for 30 min. Before spraying the solution, the substrate temperature (T<sub>S</sub>) was set at 310 °C with an accuracy of ±5 °C using a digital temperature controller for both options. Other deposition parameters such as spray deposition rate (ml/min), spray solution volume and the pressure of the carrier gas were reported in Table 1.

### 2.2 Characterization of thin films

An X-ray diffractometer (D8 Advance Bruker) was used to record X-ray diffraction (XRD) patterns using Cu-K<sub>α</sub> radiation (λ = 0.15406 nm) spectra in the 2θ range

10°–70°. Spectral transmittance and reflectance were recorded in the wavelength range 300–1100 nm by a Shimadzu UV1800 spectrophotometer. The surface morphology were investigated by using a field emission scanning electron microscope (FESEM) (Hitachi, model: S-4160). The film thickness of studied samples were determined by gravimetric weight difference method. For this, a sensitive microbalance was used and film density was assumed as the bulk density of MoO<sub>3</sub> (4.69 g/cm<sup>3</sup>).

Electrical resistivity and Hall effect data (magnetic field strength = 200 mT) of the samples were measured in the Van der Pauw configuration [12]. Finally by applying a temperature gradient between the two ends of the samples, the thermoelectric electromotive force (emf) of the prepared films were measured, and then the Seebeck coefficients were determined by calculating the slope of the thermoelectric emf versus temperature difference.

## 3 Results and discussion

### 3.1 Structural properties

Figure 1 shows the X-ray diffraction spectra of pure and Sulfur content MoO<sub>3</sub> films deposited at substrate temperature of 310 °C. The pure MoO<sub>3</sub> thin film (MO) shows the single orthorhombic phase (α-MoO<sub>3</sub>) (JCPDS Card No. 075-0912) with preferred orientation along (020) direction. With increasing the mole concentration ratio of [S]/[Mo], the grown samples show not only the MoO<sub>3</sub> orthorhombic structure characteristic peaks of (020), (040), (060) and (0100), but also traces of MoS<sub>2</sub> hexagonal structure (JCPDS Card No. 14-0072) with (300), (200), (210), (400) and (420) directions in films (Fig. 1). The low intensity of XRD patterns at higher S-content films suggests the possibility of amorphous phases being present in the studied samples. According to ionic radius values of O<sup>2-</sup> (r = 1.32 Å) and S<sup>2-</sup> (r = 1.82 Å), it can be concluded that as the sulfur concentration increases in the layers, they substitute in the oxygen lattice sites and therefore the MoS<sub>2</sub> phase forms in higher S- containing MoO<sub>3</sub> films. Also, the d<sub>hkl</sub> experimental values for samples were compared with data (from JCPDS Card Nos: 075-0912 and 14-0072); and

**Table 1** The chemical deposition parameters for the studied samples prepared by spray pyrolysis technique

Sample	T <sub>S</sub> (°C)	[S]/[Mo] molar ratio	Spray volume (ml)	Spray rate (ml/min)	P (bar)
MO	310	0	50	10	3
MOS-4	310	4	50	10	3
MOS-6	310	6	50	10	3
MOS-8	310	8	50	10	3
MOS-10	310	10	50	10	3

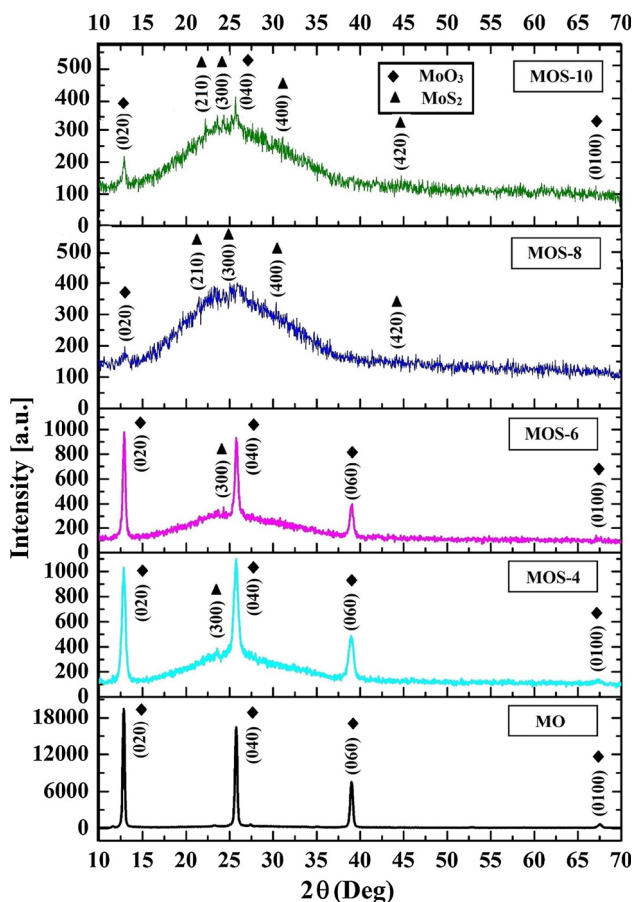


**Fig. 1** XRD pattern of pure MoO<sub>3</sub> thin film and Sulfur content MoO<sub>3</sub> thin films

were found to be in good agreement with the standard values as shown in Table 2.

The crystallite size (*D*) for the preferred orientation along (020) direction in these films is determined using Scherer’s formula:

$$D = \frac{k\lambda}{\delta w \cos \theta} \tag{3}$$

where  $\lambda$  is the X-ray wavelength,  $\delta w$  is the full-width at half-maximum of the main peak,  $k$  is a constant (close to unity) and  $\theta$  is the Bragg angle. The results of these calculations are listed in Table 3. The variation of the crystallite size has major influence on optical and electrical properties of the samples, as described in the following.

### 3.2 Morphological properties

In order to study the surface morphology, the produced films were examined by FESEM, see Fig. 2. According to high magnification of these images (Fig. 2a–e), the morphology of all samples are branch-like with a large amount of porosity. The low magnification image of a typical sample (MOS-4 sample), (Fig. 2f), shows that the product consist of a sponge-type structure and the sponge is composed of cubic nanoparticles, see Fig. 2g. The average diameter of the cubic nanoparticles, by which the sponge is made, was found to be in the range 50–200 nm and is evident from the low magnification image of this sample.

### 3.3 Optical properties

The optical transmittance (*T*) and reflectance (*R*) of the films as a function of wavelength are shown in Fig. 3. These graphs show that reflectance of the samples has a very small spectral dependence, with a low (~0.5–4 %) reflectivity in the UV–Vis–NIR wavelength regions. The transmittance results show that pure MoO<sub>3</sub> thin film (sample MO), exhibited a nearly sharp fall in the transmittance near the fundamental absorption, while those layers containing sulfur exhibited the presence of shoulders in the transmission spectra. The existence of shoulders near the fundamental absorption indicated the presence of

**Table 2** Comparison of observed “d” values, obtained from XRD data of samples prepared at various [S]/[Mo] molar ratio, with the standard “d” values

Sample	MO	MOS-4	MOS-6	MOS-8	MOS-10	MoO <sub>3</sub> (JCPDC Card No: 075-0912) MoS <sub>2</sub> (JCPDC Card No: 14-0072)	
						(hkl)-phase	Standard d <sub>hkl</sub> values
2θ (°) ↓	d <sub>hkl</sub> (Å) (realized)						
12.69	6.88	6.91	6.86	6.81	6.90	(020)-Orthorhombic	6.97
22.06	–	–	–	4.15	4.02	(210)-Hexagonal	4.02
25.05	–	3.77	3.66	3.56	3.67	(300)-Hexagonal	3.55
25.53	3.45	3.46	3.46	3.43	3.47	(040)-Orthorhombic	3.48
33.62	–	–	–	2.94	2.88	(400)-Hexagonal	2.89
38.72	2.30	2.30	2.31	–	–	(060)-Orthorhombic	2.32
44.99	–	–	–	2.03	2.04	(420)-Hexagonal	2.01
67.08	1.38	1.39	1.38	–	–	(0100)-Orthorhombic	1.39

**Table 3** The crystallite size values of the studied films for the preferred orientation along (020) direction

Sample	[S]/[Mo] molar ratio	<i>D</i> (nm)
MO	0	33.83
MOS-4	4	20.33
MOS-6	6	25.37
MOS-8	8	25.45
MOS-10	10	33.86

different phases in the layers well matched with XRD analysis (Fig. 1).

The absorption coefficient ( $\alpha$ ) of the films was evaluated from the optical transmittance and reflectance data using the formula [13]:

$$\alpha = \frac{1}{d} \ln \left( \frac{(1-R)^2}{T} \right) \quad (4)$$

where  $d$ , is the thickness of layers which are listed in Table 4. These samples presented high absorption coefficient values greater than  $10^4 \text{ cm}^{-1}$  in the visible region (Fig. 4). The absorption coefficient ( $\alpha$ ) is related to the

incident photon energy ( $h\nu$ ) by the following equation [14, 15]:

$$(\alpha h\nu)^{1/n} = A(h\nu - E_g) \quad (5)$$

where  $A$  is a constant and the exponent  $n$  depends on the type of transition,  $n = 1/2$  and  $2$  for direct and indirect transitions, respectively. Since  $\text{MoO}_3$  is well established as a direct band gap semiconductor [7, 8], we can evaluate  $E_g$ , from the plot of  $(\alpha h\nu)^2$  versus  $h\nu$ . The details of analysis of the direct band gaps can be found in the inset of the related graph, see Fig. 4.

The  $E_g$  value of MO sample (pure  $\text{MoO}_3$  film) was found to be 3.05 eV (inset of Fig. 4a). For those layers containing sulfur it had been observed that the plots were parabolic in nature, having two distinct inflexions which indicates two transitions occurring in sulfur content  $\text{MoO}_3$  thin films. The band gap energy ( $E_g$ ) calculations revealed that these phases were correspond to  $\text{MoO}_3$  and  $\text{MoS}_2$ . For each sample, both the band gaps are comparable with the reported values, i.e. 3.14–3.65 eV [7, 8, 16] for  $\text{MoO}_3$  and with the normal value, i.e. 1.8 eV for  $\text{MoS}_2$  [17]. Shape, size, size distribution, phase, crystalline degree, and defects can play a role in the energy gaps of materials. Generally,

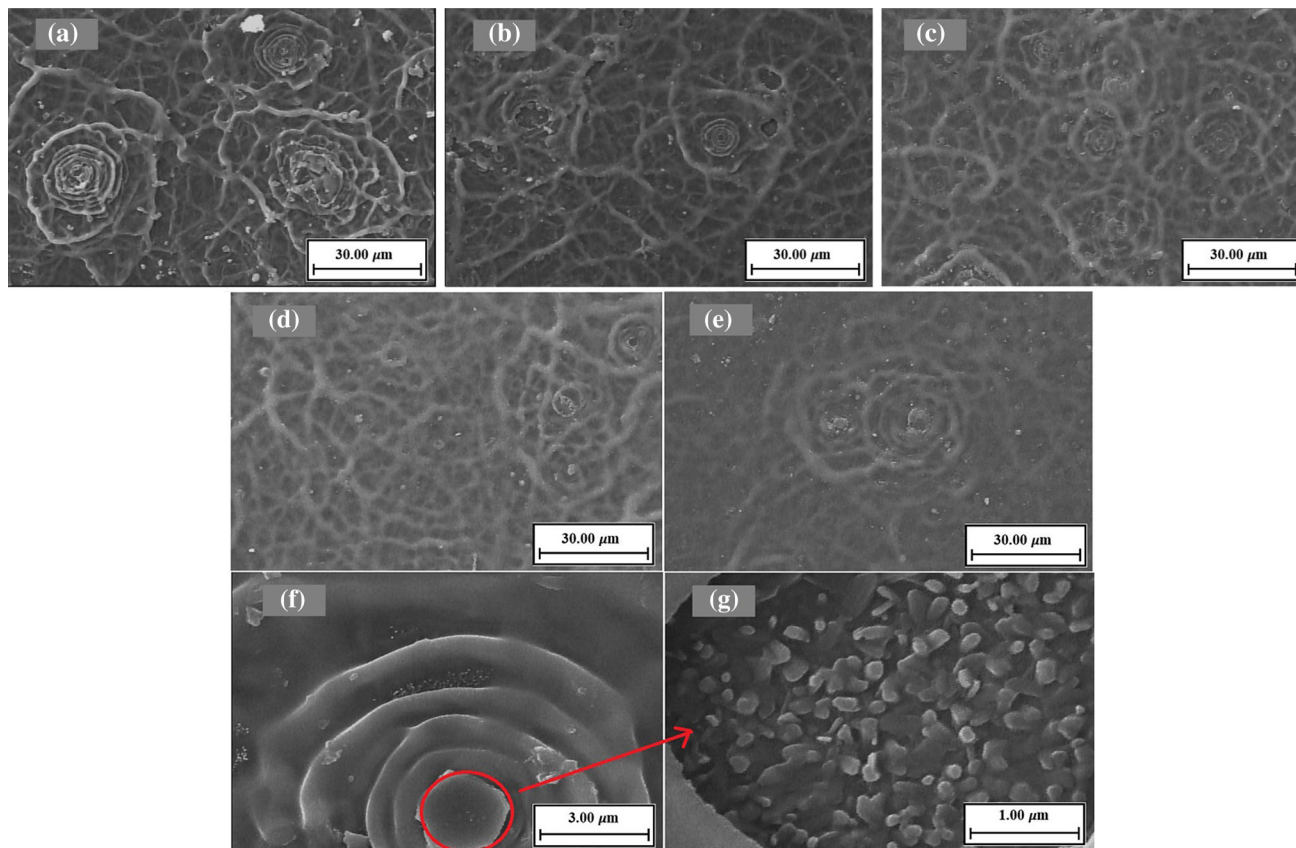


**Fig. 2** FESEM images of the studied samples with low magnification **a** MO, **b** MOS-4, **c** MOS-6, **d** MOS-8, **e** MOS-10 and high magnification image of a the typical sample (MOS-4 sample) (**f** and **g**)



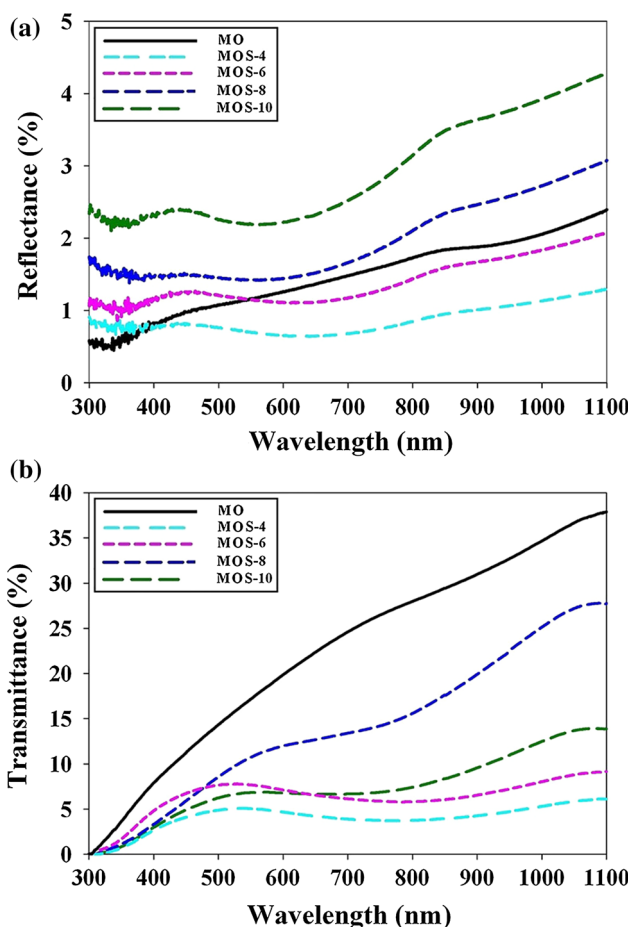


**Fig. 3** Results of transmittance and reflectance measurement of the studied samples

**Table 4** The thickness, electrical and thermoelectrical measurement results of the films for various sulfur concentration

Sample	Thickness (nm)	Resistivity ( $\Omega$ cm)	Carrier density ( $\text{cm}^{-3}$ )	Mobility ( $\text{cm}^2/\text{V s}$ )
MO	440	$\geq 50 \times 10^3$	–	–
MOS-4	418	73.41	$3.34 \times 10^{15}$	25.52
MOS-6	670	69.58	$6.99 \times 10^{15}$	12.85
MOS-8	473	70.15	$1.22 \times 10^{15}$	73.32
MOS-10	540	29.42	$1.36 \times 10^{16}$	15.64

$E_g$  becomes wider by using smaller particles but narrower by the presence of defects.

### 3.4 Electrical properties

The effect of [S]/[Mo] molar ratio on the electrical properties of the samples were evaluated by Hall effect and resistivity measurements. Through the Hall data

acquisitions we found out that all the studied samples exhibited *p*-type conductivity. The room temperature variations of Hall mobility ( $\mu$ ), carrier density (*p*) and resistivity ( $\rho$ ) against the [S]/[Mo] molar ratio, obtained from the combined measurements of resistivity and Hall coefficient, are shown in Fig. 5, and the results are given in Table 4. It can be noticed that while the [S]/[Mo] ratio of the samples increases: (1) the values of resistivity have been decreased so that MOS-10 sample presents a lower resistivity than that of other samples. These variations were compatible with the shifts in the transmittance and reflectance spectra shown in Fig. 3 in relation with their poor/rich metallic-like behavior. (2) the degenerate hole density gradually increases from  $\sim 1.2 \times 10^{15} \text{ cm}^{-3}$  in MOS-4 to about  $1.4 \times 10^{16} \text{ cm}^{-3}$  in MOS-10 sample. The exact reason for this behavior of ‘*p*’ is not known but this might be understood as follows. It is a well-known fact that the various factors, such as crystallinity, morphology, roughness, porosity, stress, composition, film-substrate interface, etc., play a crucial role in determining the electrical properties of the films. Hence, the variation in the electrical parameters of the films reported in the present study, with respect to S to Mo molar ratio, might be attributed to the difference in their structural properties as examined by XRD.

### 3.5 Thermoelectrical properties

Figure 6 presents the variation of the thermoelectric e.m.f versus temperature difference ( $\delta T$ ) for three typical samples. It can be seen that thermoelectric e.m.f. of films is increased with increasing the temperature difference between the hot and cold sides. Also, it should be mentioned that the highest thermoelectric e.m.f. was obtained for MOS-10 sample with highest sulfur content. The explanation for increasing thermoelectric behavior is either through increased mobility and/or majority carrier concentration with increasing temperature [18]. Since it is likely that mobility does not increase due to probable thermal scattering, we believe the increased thermoelectric behavior is due to ionization of additional majority carriers in these films.

The variations of Seebeck coefficients as a function of temperature for these samples are shown in Fig. 7. Variation of Seebeck coefficient at low temperatures is nearly nonlinear, which increases very slow with a linear behavior with increasing temperature higher than 330 K. The non-linear manner in temperatures below 330 K is related to the electron-phonon and phonon-phonon interactions, while slow linear variations are related to free electron model which are temperature dependent phenomena [19]. The maximum value of Seebeck coefficient obtained in the

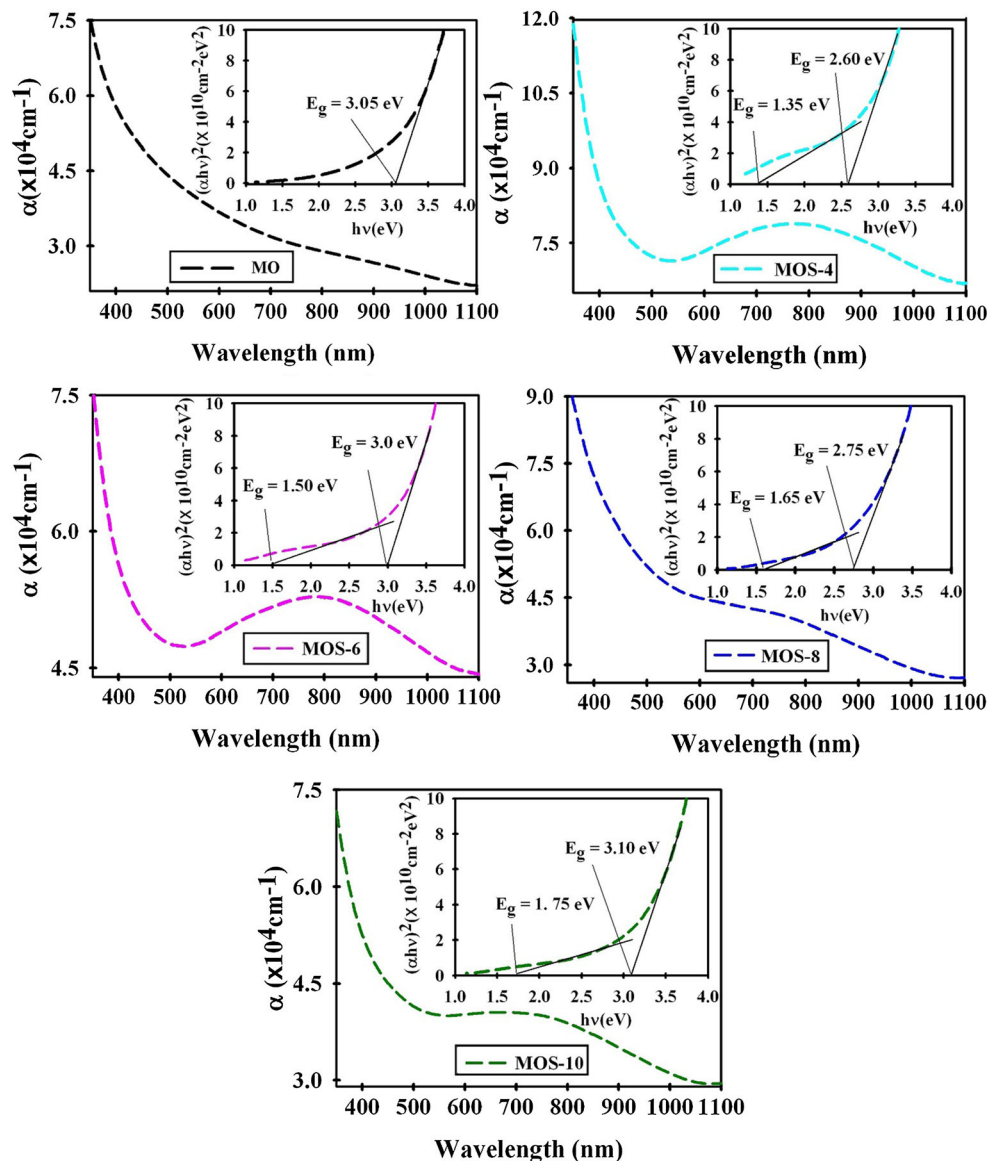


**Fig. 4** The optical absorption coefficient,  $\alpha(\lambda)$ , for pure  $\text{MoO}_3$  and Sulfur content  $\text{MoO}_3$  thin films. (inset: band gap photon energy,  $E_g$ )

present work was found to be equal to  $169 \mu\text{V/K}$  (at  $T = 360 \text{ K}$ ) for MOS-8 film.

#### 4 Conclusions

Sulfur content  $\text{MoO}_3$  thin films have been grown by the spray pyrolysis technique with different  $[\text{S}]/[\text{Mo}]$  molar ratios (0–10 at.%) on glass substrates at  $310^\circ\text{C}$ , in various aqueous solutions of ammonium molybdate tetrahydrate and thiourea. Structural, morphological, optical, electrical and thermoelectrical characterizations were performed. We found that as the  $[\text{S}]/[\text{Mo}]$  ratio increased: (1) the samples show not only the  $\text{MoO}_3$  orthorhombic structure, but also

traces of  $\text{MoS}_2$  hexagonal structure; (2) FESEM images show a sponge-type porous structure and cubic nanoparticles of nanometric dimensions; (3) the layers exhibit two distinct inflexions indicative two transitions in the plot of  $(\alpha hv)^2$  vs.  $hv$ , with evaluated  $E_g$  values of  $\sim 2.60\text{--}3.10$  and  $\sim 1.35\text{--}1.75 \text{ eV}$  correspond to  $\text{MoO}_3$  and  $\text{MoS}_2$  phases, respectively; (4) samples have a degenerate p-type conductivity with a carrier density of about  $10^{15}\text{--}10^{16} \text{ cm}^{-3}$  which increase with the increment of the sulfur concentration; (5) The thermoelectric measurements showed that the maximum value of Seebeck coefficient obtained in the present work was found to be equal to  $-169 \mu\text{V/K}$  (at  $T = 360 \text{ K}$ ) for  $\text{MoO}_3$  thin film with  $[\text{S}]/[\text{Mo}]$  molar ratio equal to 8 at.% in the spray solution.

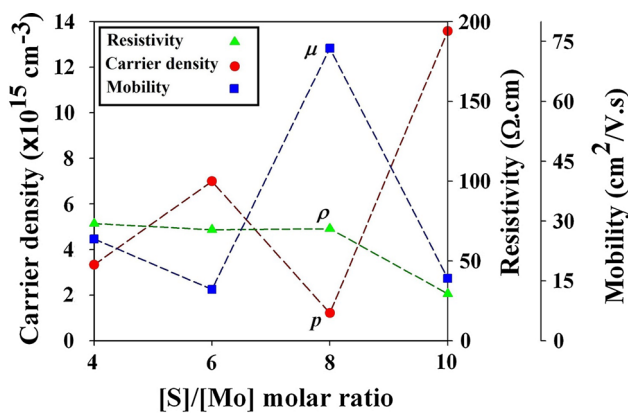


Fig. 5 The variations of resistivity  $\rho$ , hole mobility  $\mu_p$  and hole density  $p$  as a function of [S]/[Mo] ratio in the S-content MoO<sub>3</sub> thin films

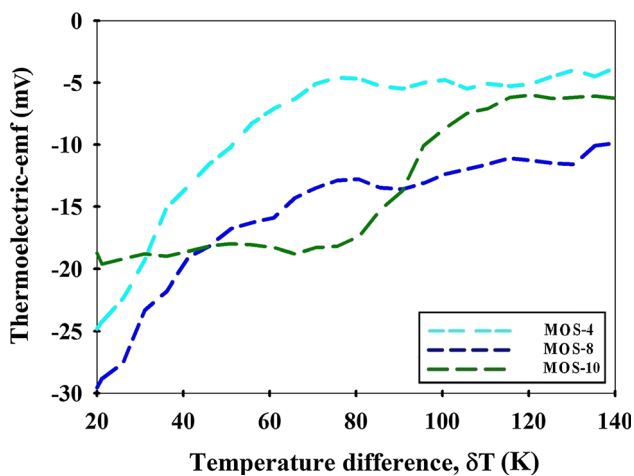


Fig. 6 Thermoelectric e.m.f versus temperature difference for the three typical samples

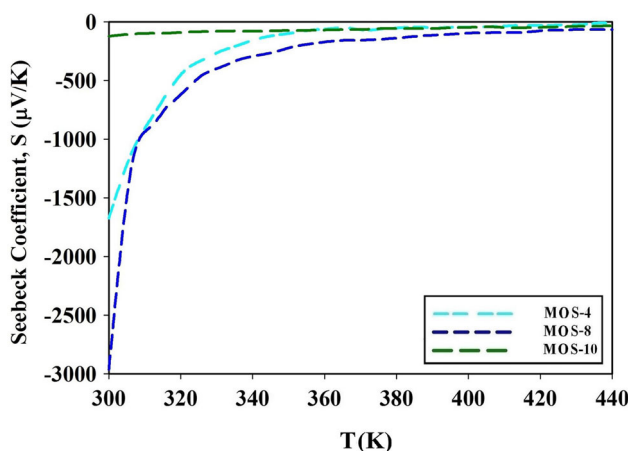


Fig. 7 Seebeck coefficient versus temperature for the three typical samples

## References

1. S.S. Mahajan, S.H. Mujawar, P.S. Shinde, A.I. Inamdar, P.S. Patil, Int. J. Electrochem. Sci. **3**, 953 (2008)
2. V. Bhosale, A. Tiwari, J. Narayan, J. Appl. Phys. **97**, 083539 (2005)
3. W. Li, F. Cheng, Z. Tao, J. Chen, J. Phys. Chem. B **110**, 119 (2006)
4. M.S. Wittingham, Proc. Solid State Chem. **12**, 41 (1978)
5. S.K. Deb, Proc. R. Soc. Lond. Ser. A **304**, 211 (1968)
6. A. Abdellaoui, G. Lévêque, A. Donnadiou, A. Bath, B. Bouchikhi, Thin Solid Films **304**, 39 (1997)
7. A. Bouzidi, N. Benramdane, H. Tabet-Derraz, C. Mathieu, B. Khelifa, R. Desfeux, Mater. Sci. Eng. B **97**, 5 (2003)
8. H.M. Martínez, J. Torres, L.D. López-Carreño, M.E. Rodríguez-García, J. Supercond. Nov. Magn. **26**, 2485 (2013)
9. A. Guerfi, L.H. Dao, J. Electrochem. Soc. **136**, 2435 (1989)
10. C. Julien, B. Yebka, G.A. Nazri, Mater. Sci. Eng. B **38**, 65 (1996)
11. R. Yousefi, B. Kamaluddin, Solid State Sci. **12**, 252 (2010)
12. L.J. Van der Pauw, Philips Res. Rep. **13**, 1 (1958)
13. P.K. Manoj, B. Joseph, V.K. Vaidyan, D. Sumangala Devi Amma, Ceram. Int. **33**, 273 (2007)
14. J.I. Pankove, *Optical Processes in Semiconductors* (Prentice-Hall, Englewood Cliffs, 1971)
15. M.A. Butler, J. Appl. Phys. **48**, 1914 (1977)
16. A. Chithambararaj, A.C. Bose, J. Alloys Compd. **509**, 8105 (2011)
17. A. Splendiani, L. Sun, Y. Zhang, T. Li, J. Kim, C.Y. Chim, G. Galli, F. Wang, Nano Lett. **10**, 1271 (2010)
18. P.S. Patil, L.D. Kadam, Appl. Surf. Sci. **199**, 211 (2002)
19. M.-M. Bagheri-Mohagheghi, N. Shahtahmasebi, M.R. Alinejad, A. Youssefi, M. Shokooh-Saremi, Solid State Sci. **11**, 233 (2009)